Proceedings of the ASME 2019 International Design Engineering Technical Conferences & Computers and Information in Engineering Conference
IDETC/CIE 2019
August 18-August 21, 2019, Anaheim, USA

IDETC2019-97486

INTEGRATED ORIGAMI-STRING SYSTEM

Ke Liu *
Department of Mechanical and Civil Engineering
California Institute of Technology
Pasadena, California, 91125
Email: liuke@caltech.edu

Madelyn Kosednar
School of Mechanical Engineering
Georgia Institute of Technology
Atlanta, Georgia, 30332
Email: madelyn.kosednar@gatech.edu

Tomohiro Tachi
Graduate School of Arts and Sciences
University of Tokyo
Tokyo, Japan
Email: tachi@idea.c.u-tokyo.ac.jp

Glaucio H. Paulino
School of Civil and Environmental Engineering
Georgia Institute of Technology
Atlanta, Georgia, 30332
Email: paulino@gatech.edu

ABSTRACT

Origami-inspired mechanical systems are mostly composed of two-dimensional elements, a feature inherited from paper folding. However, do we have to comply with this restriction on our design space? Would it be more approachable to achieve desired performance by integrating elements of different abstract dimensions? In this paper, we propose an integrated structural system consisting of both two-dimensional and one-dimensional elements. We attach elastic strings onto an origami design to modify its mechanical behavior and create new features. We show that, by introducing elastic strings to the recently proposed Morph pattern, we can obtain bistable units with programmable energy landscape. The behavior of this integrated origami-string system can be described by an elegant formulation, which can be used to explore its rich programmability.

INTRODUCTION

Origami-inspired designs are a rich source of interdisciplinary inspiration for creating multi-functional structures and programmable metamaterials [1–12]. For instance, in aerospace engineering, origami is used to make deployable solar arrays [13,14]. Inspired by origami kinematics, a new paradigm of manufacturing has been proposed to fabricate complex shell architectures of single crystal silicon at a micro scale level [15]. Beyond single layer sheets, origami assemblages have led to novel designs of functional metamaterials [1,2]. For instance, origami-inspired designs can be used as biomedical devices, such as coronary stent [16]. Moreover, automobiles equipped with origami crashboxes are effective in absorbing energy and thus protecting lives [17].

The original mathematical definition of origami is restricted to isometric transformation of simply connected developable surfaces. In recent years, advances in origami mathematics and computation technologies elevated the design of origami to a new level of complexity [18, 19], which contributed to bring origami to the attention of scientists and engineers. Within the framework of origami engineering, the concept of origami is broadened to include various morphing structures. Topologically, some of them are non-developable [20], some of them possess genus [10, 11], some of them are not simply connected (i.e. kirigami) [21, 22], and some of them even become pseudo-manifolds [2]. Yet, they are still composed of solely 2-dimensional elements, which might be an unnecessary constraint in our design space

*Address all correspondence to this author.

for engineering applications, as discussed below.

In this paper, we explore the possibility of integrating origami with elastic strings to create a hybrid cellular system composed of both two-dimensional and one-dimensional elements. Previous attempts [23,24] use strings with origami to control their geometries. Here we adopt strings in origami structures for control of mechanical properties, and in particular, bistability. Our integrated string-origami system is constructed based on the recently proposed Morph pattern [25], which is a periodic origami pattern with a non-developable degree-4 unit cell. Through analytical and numerical analyses, we demonstrate that the attachment of strings to the Morph pattern leads to programmable bistability and multistability of the new integrated system, while preserving the features of the original Morph pattern, such as tunable Poisson's ratio over a wide range of negative to positive values, and topological mode-locking [25].

DESIGN OF AN ORIGAMI-STRING UNIT CELL

The origami part of the system is based on the Morph pattern, which consists of two identical pairs of parallelogram panels, as shown in Fig. 1. Similarly to the original Morph pattern [25], the two pairs of identical panels lead to one plane of symmetry. The panel shapes are defined by the angles α, β, and edge lengths a, b, c. To describe the folding of the origami pattern, we denote angles ψ and ϕ $(=\phi_R+\phi_F)$ as the angles between opposite creases, and γ_1 to γ_4 as the dihedral angles between panels (see Fig. 1). To ensure that the unit cell has an orthorhombic bounding box, the edge lengths a and b become functions of each other, such that,

$$\frac{a}{b}=\left|\frac{\cos\phi_R}{\cos\phi_F}\right| . \tag{1}$$

According to the symmetry of the unit cell, we obtain:

$$\cos\alpha=\cos\frac{\psi}{2}\cos\phi_F, \tag{2}$$

$$\cos\beta=\cos\frac{\psi}{2}\cos\phi_R. \tag{3}$$

We can see that the ratio between a and b becomes:

$$\frac{a}{b}=\left|\frac{\cos\beta}{\cos\alpha}\right| , \tag{4}$$

which is a constant for a design with given α and β angles, and does not depend on the folding of the origami pattern. Therefore, we may choose the independent design variables for the origami part of the design to be α, β, a, and c.

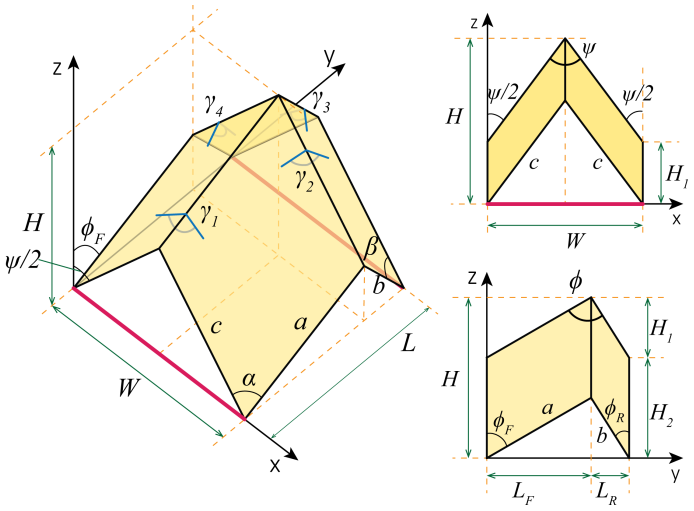

FIGURE 1. DESIGN OF A UNIT CELL OF THE INTEGRATED ORIGAMI-STRING SYSTEM. THE YELLOW SHADING DENOTES THE ORIGAMI PANELS, AND THE RED LINES DENOTE THE STRINGS. THE SUBSCRIPTS F AND R OF ϕ_F AND ϕ_R IMPLY THE RELATIVE LOCATIONS OF BEING AT THE FRONT AND RARE OF THE UNIT CELL, RESPECTIVELY.

The extrinsic length L and width W of the unit cell are then given by:

$$W=2c\sin\frac{\psi}{2}, \tag{5}$$

$$L=\sqrt{a^2+b^2-2ab\cos\phi}. \tag{6}$$

Using spherical trigonometry at the central vertex, we obtain:

$$\cos\psi=\cos^2\alpha+\sin^2\alpha\cos\gamma_1, \tag{7}$$

$$\cos\psi=\cos^2\beta+\sin^2\beta\cos\gamma_3, \tag{8}$$

$$\cos\phi=\cos\alpha\cos\beta+\sin\alpha\sin\beta\cos\gamma_2, \tag{9}$$

$$\cos\phi=\cos\alpha\cos\beta+\sin\alpha\sin\beta\cos\gamma_4. \tag{10}$$

Considering symmetry of the design, we can further derive that:

$$\cos\beta=\cos\alpha\cos\phi+\sin\alpha\sin\phi\cos\left(\frac{\gamma_1}{2}\right), \tag{11}$$

$$\cos\alpha=\cos\beta\cos\phi+\sin\beta\sin\phi\cos\left(\frac{\gamma_3}{2}\right), \tag{12}$$

$$\sin\frac{\psi}{2}=\sin\alpha\sin\frac{\gamma_1}{2}=\sin\beta\sin\frac{\gamma_3}{2}. \tag{13}$$

Rearranging the terms of Eq. (11), we obtain that:

$$\cos\gamma_1 = \frac{2(\cos\beta - \cos\alpha\cos\phi)^2}{\sin^2\alpha\sin^2\phi} - 1. \tag{14}$$

Substituting Eq. (7) into Eq. (14), the configuration space of the origami pattern (i.e. the Morph pattern [25]) is characterized by the following equation:

$$\cos\psi = \cos 2\alpha + \frac{2(\cos\beta - \cos\alpha\cos\phi)^2}{\sin^2\phi}. \tag{15}$$

The elastic strings are placed between two pairs of vertices, as shown in Fig. 1. Let us denote the unformed length of the strings as W_s. We can see that the strains in the strings are functions of the unit cell width W. When $W \leq W_s$, the strings go slack, and have negligible influence on the energetic state of the system. In this case, the behavior of the integrated string-origami system is dominated by the origami part. When $W > W_s$, the strings are under tension, and will contribute to the system energy.

CONSTITUTIVE MODEL OF ELASTIC STRINGS

In static and quasi-static analyses, a nonlinear constitutive model that expresses zero stiffness under compression can equivalently model the slackness of a string. By truncating the compressive part of a two-term Ogden type hyperelastic constitutive model [26], we can describe the behavior of the strings in our integrated system. We denote λ_1 as the principle stretch of the string, $\mathscr{W}$ as the strain energy density, ε_{xx} as the Green-Lagrange strain, and S_{xx} as the 2nd Piola-Kirchhoff stress. We can write the strain energy function of an elastic string as:

$$\mathscr{W}(\lambda_1) = \begin{cases} \frac{E_s}{\alpha_1^{OG} - \alpha_1^{OG}} \left(\frac{\lambda_1^{\alpha_1^{OG}} - 1}{\alpha_1^{OG}} + \frac{\lambda_1^{\alpha_2^{OG}} - 1}{\alpha_2^{OG}} \right), & \text{when } \lambda_1 \geq 1 \\ 0, & \text{when } \lambda_1 < 1 \end{cases}. \tag{16}$$

The above expression contains material related parameters for the Ogden model: E_s, α_1^{OG}, and α_2^{OG}. The parameter E_s is determined by the initial tangent modulus of the material (near $\lambda_1 = 1$). The parameters α_1^{OG} and α_2^{OG} reflect the nonlinear effect of the constitutive behavior of the material. In the current study, we consider $\alpha_1^{OG} = 5$ and $\alpha_2^{OG} = 1$, and the corresponding curve by Eq. (16) is plotted in Fig. 2(A). The principle stretch λ_1 equals to W/W_s. When $\lambda_1 < 1$, the string become slack (there is actually no compressive stress within the element). Therefore, compression (i.e. $\lambda_1 < 1$) causes zero strain energy.

Accordingly, the stress in the strings are always positive.

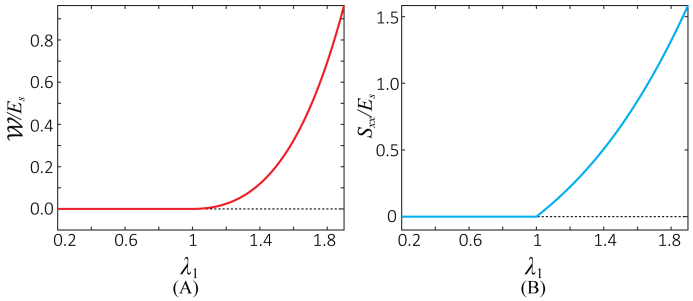

FIGURE 2. THE HYPERELASTIC CONSTITUTIVE MODEL OF STRINGS. (A) ENERGY DENSITY ($\mathscr{W}$) VS. PRINCIPLE STRETCH (λ_1). (B) STRESS (S_{xx}) VS. PRINCIPLE STRETCH (λ_1).

Given that $\varepsilon_{xx} = (\lambda_1^2 - 1)/2$, we can derive the stress S_{xx} as:

$$\begin{aligned} S_{xx} &= \frac{\partial\mathscr{W}}{\partial\varepsilon_{xx}} = \frac{\partial\mathscr{W}}{\partial\lambda_1}\frac{\partial\lambda_1}{\partial\varepsilon_{xx}} \\ &= \begin{cases} \frac{E_s}{\alpha_1^{OG} - \alpha_1^{OG}} \left(\lambda_1^{\alpha_1^{OG}-2} - \lambda_1^{\alpha_2^{OG}-2} \right), & \text{when } \lambda_1 \geq 1 \\ 0, & \text{when } \lambda_1 < 1 \end{cases}. \end{aligned} \tag{17}$$

We remark that S_{xx} is continuous but not smooth at $\lambda_1 = 1$, as shown in Fig. 2(B).

MECHANICAL BEHAVIOR

The attachment of elastic strings changes the mechanical behavior of the original origami pattern, i.e. the Morph. When the strings are slack, the properties of the Morph pattern are not affected and will be preserved. When the strings are tensioned, the behavior of the integrated system changes. In this section, we focus on the bistability of the unit cell of the integrated origami-string system, which is a new feature not associated with the original Morph origami pattern.

Theoretical Analysis Assuming Rigid Origami Kinematics

If we ignore the deformation of panels (as a simplification), the system stored energy is contributed by the elasticity of the folding hinges and the strings. Thus, we can analytically describe the system behavior in terms of its stored energy and resistance forces under deformation. We assume that the folding hinges are linear elastic, and that they have a uniform rotational modulus K_f per unit length. The initial dihedral angles are denoted as $\gamma_{i,0}$'s. We can express the total stored energy of a unit cell as:

$$U_T = \sum_{i=1}^{4} \frac{1}{2} K_f \ell_i (\gamma_i - \gamma_{i,0})^2 + A_s W_s \mathscr{W}(\lambda_1), \tag{18}$$

where ℓ_i denotes the length of a hinge (i.e. a, b, or c), and A_s is the total cross sectional area of elastic strings in a unit cell. As we assume rigid origami kinematics, the deformation of the unit cell can be described using a single degree of freedom (DOF). Taking derivative of Eq. (18), we can evaluate the resistance force when deforming the unit cell in directions W and L, respectively:

$$\begin{aligned}\frac{\mathrm{d}U_T}{\mathrm{d}W} &= \sum_{i=1,3} K_f l_i (\gamma_i - \gamma_{i,0}) \frac{\mathrm{d}\gamma_i}{\mathrm{d}\psi}\frac{\mathrm{d}\psi}{\mathrm{d}W} \\ &+ \sum_{i=2,4} K_f l_i (\gamma_i - \gamma_{i,0}) \frac{\mathrm{d}\gamma_i}{\mathrm{d}\phi}\frac{\mathrm{d}\phi}{\mathrm{d}L}\frac{\mathrm{d}L}{\mathrm{d}W} \\ &+ A_s W_s \frac{\mathrm{d}\mathscr{W}}{\mathrm{d}\lambda_1}\frac{\mathrm{d}\lambda_1}{\mathrm{d}W}, \end{aligned} \tag{19}$$

$$\begin{aligned}\frac{\mathrm{d}U_T}{\mathrm{d}L} &= \sum_{i=1,3} K_f l_i (\gamma_i - \gamma_{i,0}) \frac{\mathrm{d}\gamma_i}{\mathrm{d}\psi}\frac{\mathrm{d}\psi}{\mathrm{d}W}\frac{\mathrm{d}W}{\mathrm{d}L} \\ &+ \sum_{i=2,4} K_f l_i (\gamma_i - \gamma_{i,0}) \frac{\mathrm{d}\gamma_i}{\mathrm{d}\phi}\frac{\mathrm{d}\phi}{\mathrm{d}L} \\ &+ A_s W_s \frac{\mathrm{d}\mathscr{W}}{\mathrm{d}\lambda_1}\frac{\mathrm{d}\lambda_1}{\mathrm{d}W}\frac{\mathrm{d}W}{\mathrm{d}L}. \end{aligned} \tag{20}$$

Moreover, for the sake of completeness, we derive the following derivatives:

$$\begin{aligned}&\frac{\mathrm{d}\gamma_1}{\mathrm{d}\psi} = \frac{\sin\psi}{\sin^2\alpha\sin\gamma_1}, \frac{\mathrm{d}\gamma_3}{\mathrm{d}\psi} = \frac{\sin\psi}{\sin^2\beta\sin\gamma_3}, \\ &\frac{\mathrm{d}\gamma_2}{\mathrm{d}\phi} = \frac{\mathrm{d}\gamma_4}{\mathrm{d}\phi} = \frac{\sin\phi}{\sin\alpha\sin\beta\sin\gamma_2}, \\ &\frac{\mathrm{d}\phi}{\mathrm{d}L} = \frac{1}{ab\cos\phi}, \frac{\mathrm{d}\psi}{\mathrm{d}W} = \frac{1}{c\cos(\psi/2)}, \\ &\frac{\mathrm{d}W}{\mathrm{d}L} = \frac{4c^2L}{a^2W}\left|\frac{\cos\beta}{\cos\alpha}\right|\frac{(\cos\alpha-\cos\beta\cos\phi)(\cos\beta-\cos\alpha\cos\phi)}{\sin^4\phi}. \end{aligned} \tag{21}$$

We plot the energy profiles of the integrated system as it deforms in Fig. 3 with different string material properties E_s and original lengths W_s. We let $a = 25$ mm, and $c = 20$ mm. We consider $E_{s,0} = 12$ MPa, $\alpha_1^{OG} = 5$, $\alpha_2^{OG} = 1$, $A_s = 3$ mm^2, which are estimated from the physical model (see Section on "Demonstrative Prototypes"). The rotational modulus of folding hinges is estimated by the following formula (for a reasonable order of magnitude):

$$K_f = \frac{1.5}{a}\frac{E_p t^3}{12(1-\nu^2)}, \tag{22}$$

where $E_p = 1000$ MPa is the assumed Young's modulus of the panels, ν is the assumed Poisson's ratio that equals to 0.3, and $t =$ 0.2 mm is the approximate thickness of panels near the embossed hinge area (see Section on "Demonstrative Prototypes").

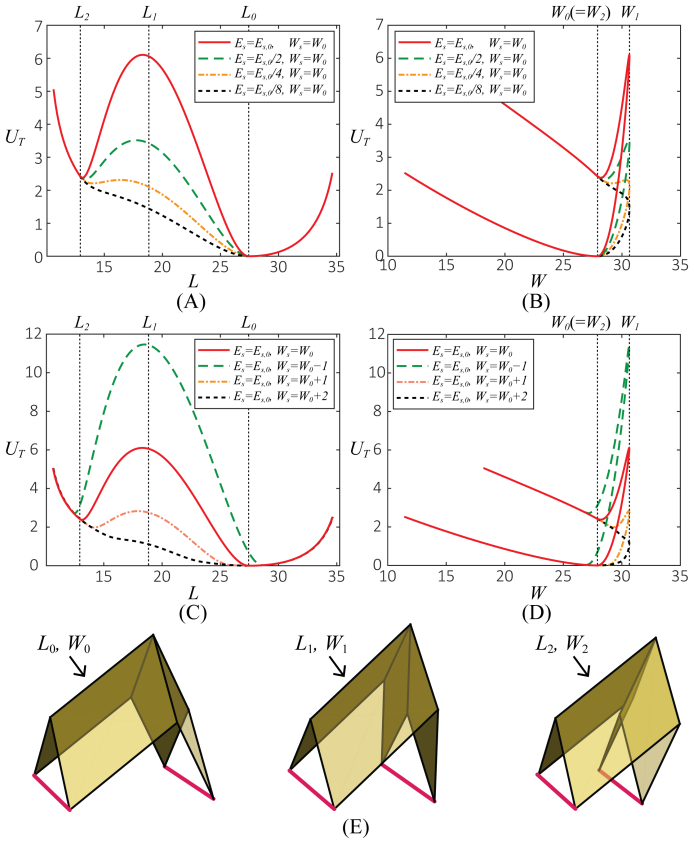

FIGURE 3. STORED ENERGY OF THE SYSTEM AT DIFFERENT CONFIGURATIONS. (A) AND (B) SHOW THE PROGRAMMABILITY OF U_T WITH RESPECT TO E_s. (C) AND (D) SHOW THE PROGRAMMABILITY OF U_T WITH RESPECT TO W_s. (E) DEMONSTRATION OF THREE KEY FRAMES DURING THE DEFORMATION PROCESS.

In Fig. 3, L_0 defines the initial projected length of the unit cell structure, and W_0 denotes the initial width. We define L_1 as the length of the structure when ψ reaches the maximum (i.e. when $\gamma_3 = \pi$), and W_1 is the corresponding width. Finally, L_2 and W_2 are measured when the unit cell is reverted such that ψ become the same as ψ_0 but the hinge γ_3 is now a valley fold, and we have $W_2 = W_0$. The corresponding configurations of the unit cell are depicted in Fig. 3(E). We remark that, owing to the interaction between the origami and the strings, this configuration of L_2 and W_2 is not at a local minimum of the energy. The actual local minimum of energy happens slightly before W_2 approaches W_0, as demonstrated in Fig. 3(A) and (B). Thus we conclude that both E_s and W_s can be used to program the energy landscape of the integrated system. Given the same rotational modulus of the hinges (i.e. K_f), a larger W_s or/and smaller E_s may result in monostable unit cells.

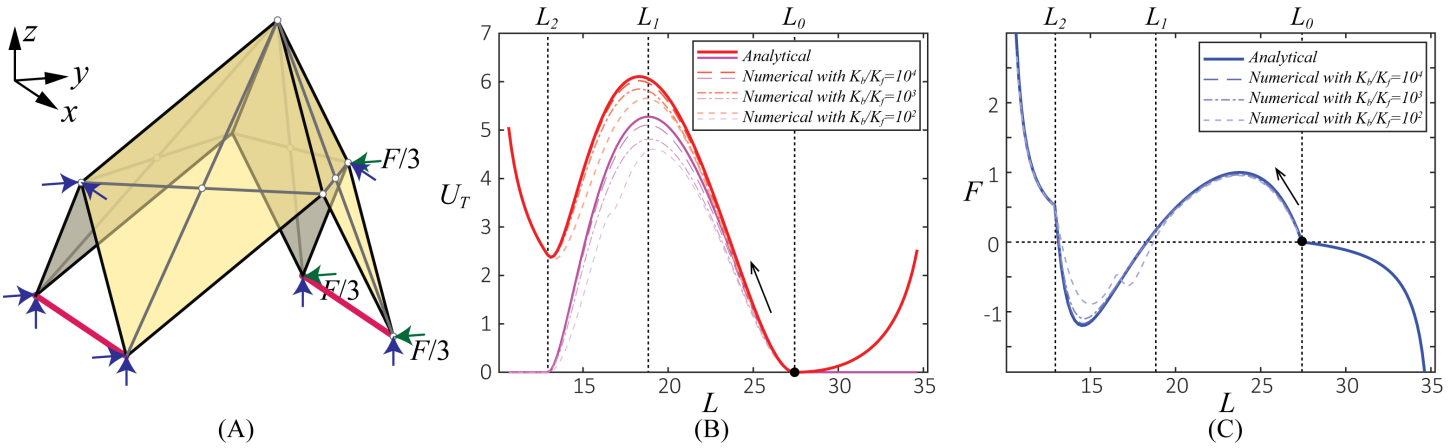

FIGURE 4. NUMERICAL ANALYSIS OF THE INTEGRATED ORIGAMI-STRING SYSTEM. (A) BOUNDARY CONDITION FOR NUMERICAL SIMULATION. (B) STORED ENERGY VS. UNIT CELL LENGTH. THE PORTION BELOW THE THINNER (PURPLE IN COLOR) CURVES ARE ENERGY STORED IN THE ELASTIC STRINGS. (C) TOTAL REACTION FORCE VS. UNIT CELL LENGTH. IN (B) AND (C), THE DOTS INDICATE THE INITIAL CONFIGURATION IN THE NUMERICAL ANALYSIS. THE ARROWS INDICATE THE LOADING DIRECTION.

Numerical Analysis Considering Compliance of Panels

In reality, the rigid origami assumption can hardly be satisfied owing to the bending, shearing, and stretching of panels. To assess the effect of the compliance of panels, we conduct numerical simulations using the MERLIN software [27], which implements the reduced order bar-and-hinge model [28–31]; and compare the results with our analytically derived predictions.

We adopt the N5B8 discretization scheme [30] such that each parallelogram panel is discretized into 4 triangles, as shown in Fig. 4(A). The material associated parameters are adopted to be the same as the basic case in the Section on "Theoretical Analysis Assuming Rigid Origami Kinematics" (i.e., $E_{s,0} = 12$ MPa and $W_s = W_0$). The non-rigid effect is accounted for by considering finite bending stiffness and stretching stiffness. Therefore, we assign Young's modulus $E_p = 1000$ MPa and area $A_p = 15$ mm^2 to the bars in the bar-and-hinge model. The bending modulus K_b is computed as multiples of K_f. The multipliers are indicated in Fig. 4(B) and (C).

The boundary condition of the simulation is illustrated in Fig. 4(A). The blue arrows indicates constraints in translation, and the green arrows indicates the applied forces. In Fig. 4(C), F is the total reaction force, in the direction indicated by the green arrows. As expected, we can see that as we increase K_b/K_f (hence approaching rigid origami assumption of panels), the curves of U_T and F get closer to the analytical prediction. The compliance of panels reduces the reaction force and stored energy of the system, as it provides more DOFs for the deformation kinematics.

DEMONSTRATIVE PROTOTYPES

Physical models are made for proof-of-concept purpose, as shown in Fig. 5. The prototype has a layered construction to best approximate rigid origami without approaching "thick origami" considerations. The base layer that serves as the foundation for the rest is made of "Durilla Durable Papers Premium Ice Paper" (CTI Paper USA Inc, Wisconsin, U.S.), which is made from a paper-film-paper lamination process. The sandwich structure of the Ice paper allows us to make flexible hinges by laser engraving, which burns out the covering vellum paper layers while leaving the plastic film layer. The particular hinge on the prototype, is 1.5mm wide with a constant 50.8 mm length, to allow extra clearance for the multi-layer construction. As the origami pattern is not developable, we need to glue the pieces into the final 3D form. All layers of the model are held together by 3M 8153LE 300LSE Eco Adhesive Sheets (3M, Minnesota, U.S.) cut to the appropriate size of the respective layers. The rigidity of the panels is imposed by covering transparent plastic sheets of thickness 0.5mm that are at 92.5% of the original panel dimensions. A final decorative layer of construction paper is added to the external faces of the Ice paper with adhesive sheets. We attach latex rubber bands (Mobilon Band 55X2X0.3, Nisshinbo, Japan) to the origami model as the elastic strings. In the future, these models will be tested experimentally.

OUTLOOK

In this paper, we propose an integrated origami-string system by attaching elastic strings to the Morph origami pattern. The resultant system has unit cells with programmable energy landscape that can accommodate for bistable snapping, which is a new fea-

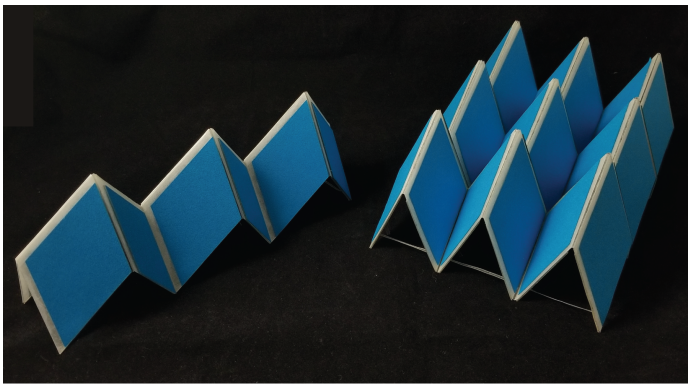

(A)

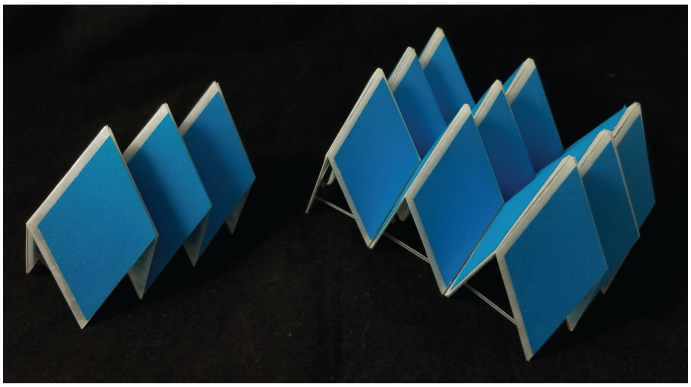

(B)

FIGURE 5. PHOTOS OF PHYSICAL PROTOTYPES. (A) TWO MODELS IN STABLE EXPANDED STATES. (B) TWO MODELS IN STABLE REVERTED STATES.

ture compared to the Morph pattern. In the meantime, the kinematics of the Morph pattern is not significantly affected, and thus the integrated system can also achieve tunable Poisson's ratio over a wide range of negative to positive values, and other properties of the original Morph pattern such as topological mode-locking [25].

Moving forward, we foresee this integrated origami-string system to inspire a new avenue beyond conventional origami designs towards reconfigurable structures and programmable metamaterials. The idea of attaching elastic strings to known origami designs can be explored for other patterns, with the potential to alter and enhance the original origami systems for better mechanical performance as required for engineering applications.

ACKNOWLEDGMENT

We thank the support from the US National Science Foundation (NSF) through grant no.1538830, the Raymond Allen Jones Chair at Georgia Tech, and the China Scholarship Council (CSC).

REFERENCES

[1] Schenk, M., and Guest, S. D., 2013. "Geometry of Miura-folded metamaterials". *Proceedings of the National Academy of Sciences,* ***110***(9), pp. 3276–3281.

[2] Filipov, E. T., Tachi, T., and Paulino, G. H., 2015. "Origami tubes assembled into stiff, yet reconfigurable structures and metamaterials". *Proceedings of the National Academy of Sciences*, p. 201509465.

[3] Yasuda, H., and Yang, J., 2015. "Reentrant origami-based metamaterials with negative poisson's ratio and bistability". *Physical Review Letters,* ***114***, p. 185502.

[4] Li, S., Fang, H., and Wang, K. W., 2016. "Recoverable and programmable collapse from folding pressurized origami cellular solids". *Physical Review Letters,* ***117***, p. 114301.

[5] Wei, Z. Y., Guo, Z. V., Dudte, L., Liang, H. Y., and Mahadevan, L., 2013. "Geometric mechanics of periodic pleated origami". *Physical Review Letters,* ***110***(21), pp. 1–5.

[6] Boatti, E., Vasios, N., and Bertoldi, K., 2017. "Origami metamaterials for tunable thermal expansion". *Advanced Materials,* ***29***(26), p. 1700360.

[7] Silverberg, J. L., Evans, A. A., McLeod, L., Hayward, R. C., Hull, T., Santangelo, C. D., and Cohen, I., 2014. "Using origami design principles to fold reprogrammable mechanical metamaterials". *Science,* ***345***(6197), pp. 647–650.

[8] Rogers, J., Huang, Y., Schmidt, O. G., and Gracias, D. H., 2016. "Origami MEMS and NEMS". *MRS Bulletin,* ***41***(2), p. 123–129.

[9] Dudte, L. H., Vouga, E., Tachi, T., and Mahadevan, L., 2016. "Programming curvature using origami tessellations". *Nature Materials,* ***15***(5), p. 583.

[10] Overvelde, J. T., de Jong, T. A., Shevchenko, Y., Becerra, S. A., Whitesides, G. M., Weaver, J. C., Hoberman, C., and Bertoldi, K., 2016. "A three-dimensional actuated origami-inspired transformable metamaterial with multiple degrees of freedom". *Nature Communication,* ***7***, p. 10929.

[11] Overvelde, J. T. B., Weaver, J. C., Hoberman, C., and Bertoldi, K., 2017. "Rational design of reconfigurable prismatic architected materials". *Nature,* ***541***, pp. 347–352.

[12] Pinson, M. B., Stern, M., Ferrero, A. C., Witten, T. A., Chen, E., and Murugan, A., 2017. "Self-folding origami at any energy scale". *Nature Communication,* ***8***, p. 15477.

[13] Miura, K., 1985. Method of Packaging and Deployment of Large Membranes in Space. Tech. rep., Institute of Space and Astronautical Science.

[14] Lang, R. J., Magleby, S., and Howell, L. L., 2015. "Single-degree-of-freedom rigidly foldable cut origami flashers". *Journal of Mechanisms and Robotics,* ***8***, p. 031005.

[15] Zhang, Y., Yan, Z., Nan, K., Xiao, D., Liu, Y., Luan, H., Fu, H., Wang, X., Yang, Q., Wang, J., Ren, W., Si, H., Liu, F., Yang, L., Li, H., Wang, J., Guo, X., Luo, H., Wang, L., Huang, Y., and Rogers, J. A., 2015. "A mechanically

driven form of Kirigami as a route to 3D mesostructures in micro/nanomembranes". *Proceedings of the National Academy of Sciences,* ***112***(38), p. 201515602.

[16] Kuribayashi, K., Tsuchiya, K., You, Z., Tomus, D., Umemoto, M., Ito, T., and Sasaki, M., 2006. "Self-deployable origami stent grafts as a biomedical application of Ni-rich TiNi shape memory alloy foil". *Materials Science and Engineering A,* ***419***(1-2), pp. 131–137.

[17] Ma, J., and You, Z., 2013. "Energy Absorption of Thin-Walled Square Tubes With a Prefolded Origami Pattern — Part I : Geometry and Numerical Simulation". *Journal of Applied Mechanics,* ***81***(January 2014), pp. 1–11.

[18] Lang, R. J., 2011. *Origami Design Secrets*, 2nd ed. CRC Press.

[19] Tachi, T., 2010. "Origamizing polyhedral surfaces". *IEEE Transactions on Visualization and Computer Graphics,* ***16***(2), pp. 298–311.

[20] Nassar, H., Lebée, A., and Monasse, L., 2017. "Curvature, metric and parametrization of origami tessellations: theory and application to the eggbox pattern". *Proceedings of the Royal Society A,* ***473***(2197), p. 20160705.

[21] Eidini, M., and Paulino, G. H., 2015. "Unraveling metamaterial properties in zigzag-base folded sheets". *Science Advances,* ***1***(8), pp. e1500224–e1500224.

[22] Rafsanjani, A., and Bertoldi, K., 2017. "Buckling-induced kirigami". *Physical Review Letters,* ***118***(8), p. 084301.

[23] Kilian, M., Monszpart, A., and Mitra, N. J., 2017. "String actuated curved folded surfaces". *ACM Transactions on Graphics,* ***36***(3), p. 25.

[24] Magliozzi, L., Micheletti, A., Pizzigoni, A., and Ruscica, G., 2017. "On the design of origami structures with a continuum of equilibrium shapes". *Composite Part B,* ***115***, pp. 144–150.

[25] Pratapa, P. P., Liu, K., and Paulino, G. H., 2019. "Geometric mechanics of origami patterns exhibiting Poisson's ratio switch by breaking mountain and valley assignment". *Physical Review Letters*. Accepted.

[26] Ogden, R. W., 1997. *Non-Linear Elastic Deformations*. Dover Publications, New York.

[27] Liu, K., and Paulino, G. H., 2018. "Highly efficient nonlinear structural analysis of origami assemblages using the MERLIN2 software". In *Origami 7*. Tarquin.

[28] Schenk, M., and Guest, S. D., 2011. "Origami folding: A structural engineering approach". In *Origami 5*, P. Wang-Iverson, R. J. Lang, and M. Yim, eds. CRC Press, pp. 293–305.

[29] Liu, K., and Paulino, G. H., 2016. "MERLIN : A MATLAB implementation to capture highly nonlinear behavior of non-rigid origami". In Proceedings of the IASS Annual Symposium, K. Kawaguchi, M. Ohsaki, and T. Takeuchi, eds.

[30] Filipov, E. T., Liu, K., Tachi, T., Schenk, M., and Paulino, G. H., 2017. "Bar and hinge models for scalable analysis of origami". *International Journal of Solids and Structures,* ***124***, pp. 26–45.

[31] Liu, K., and Paulino, G. H., 2017. "Nonlinear mechanics of non-rigid origami: an efficient computational approach". *Proceedings of the Royal Society A,* ***473***, p. 20170348.